

OFF-AXIS POINT SPREAD FUNCTION AND EFFICIENCY FOR ADAPTIVE OPTICS AT SAN PEDRO MÁRTIR AND OTHER SITES

V. G. Orlov,¹ L. J. Sánchez,¹ R. Avila,² and V. V. Voitsekhovich¹

RESUMEN

Estimamos la eficiencia de corrección para sistemas astronómicos de óptica adaptativa fuera de eje a partir de cuatro perfiles de C_n^2 obtenidos en cuatro sitios astronómicos: Observatorio Europeo Austral en Paranal, Chile; Observatorio de Roque de los Muchachos, Islas Canarias, Observatorio Astronómico Nacional en San Pedro Mártir, México y Observatorio de Haute Provence, Francia. Esta eficiencia se calcula a través del cociente de Strehl de la imagen corregida en las bandas V, J y K y para telescopios de la clase de 8-m. También realizamos un análisis detallado de la anisotropía de la función de distribución de punto en posiciones fuera del eje de corrección de sistemas de óptica adaptativa para el caso del sitio de San Pedro Mártir. Los perfiles de C_n^2 usados en este trabajo fueron obtenidos con globos instrumentados y con un Scidar Generalizado.

ABSTRACT

The efficiency of off-axis adaptive optics systems is estimated for four C_n^2 profiles obtained at four astronomical sites, respectively: European Southern Observatory in Paranal, Chile; Observatorio de Roque de los Muchachos, Canary Islands, Observatorio Astronómico Nacional at San Pedro Mártir, México; and Observatoire de Haute Provence, France. The efficiency of interest is considered through the Strehl ratio of the corrected image calculated for V, J and K bands and for 8-m class telescopes. A detailed analysis of anisotropy in the point spread function associated with off-axis adaptive astronomical correction is presented for the San Pedro Mártir site. The experimental C_n^2 profiles used for the calculations have been measured using instrumented balloon flights and the Generalized Scidar.

Key Words: ATMOSPHERIC EFFECTS — INSTRUMENTATION: ADAPTIVE OPTICS — METHODS: DATA ANALYSIS — SITE TESTING — TELESCOPES

1. INTRODUCTION

Off-axis adaptive optics (AO) correction is a fundamental problem for observational astronomy because it allows to improve the image quality in wide-field observations. It is known that the efficiency of off-axis correction decreases with the increase of the angular separation between the guide and observed objects, because the light from these objects passes through different paths in the turbulent atmosphere. As a result, the point spread function (PSF) associated with off-axis adaptive correction is anisotropic. This effect induces considerable distortions in wide-field images obtained with astronomical adaptive systems. It has been proved experimentally (Close *et al.* 1998) and theoretically (Voitsekhovich & Bara 1999; Fusco *et al.* 2000) that the AO PSF changes depend strongly on parameters such as telescope size, star separation, wavelength, adaptive system parameters, and turbulence conditions. In order to successfully analyze these images one requires to

use post-processing techniques for the image restoration. A key part of this procedure is the PSF. Because the AO PSF is strongly field dependent it has to be investigated as a function of the field positions for a given C_n^2 profile.

In this paper we estimate and compare the efficiency of off-axis adaptive correction for four different sites: Observatorio Astronómico Nacional at San Pedro Mártir (OAN-SPM) in Baja California, México; European Southern Observatory in Paranal, Chile; Observatorio de Roque de los Muchachos (ORM), Canary Islands, Spain and Observatoire de Haute Provence (OHP), France. Furthermore, a detailed analysis of the AO PSF is presented for the OAN-SPM site alone. We used the median C_n^2 profile obtained with a Generalized Scidar (Avila *et al.* 1998) for modeling AO PSF and also instrumented balloons data for the calculation of the efficiency.

2. THEORETICAL BACKGROUND

The long-exposure PSF, $P(\mathbf{r})$, of an off-axis observed star for a perfect on-axis adaptive correction can be written as (Voitsekhovich & Bara 1999):

¹Instituto de Astronomía, UNAM, CU, México.

²Centro de Radioastronomía y Astrofísica, UNAM, Morelia, México

$$\begin{aligned}
P(\mathbf{r}) &= \left(\frac{kA}{2\pi f}\right)^2 \frac{D^2}{2} \\
&\times \int_0^D d\rho \rho \left[\arccos\left(\frac{\rho}{D}\right) - \frac{\rho}{D} \sqrt{1 - \frac{\rho^2}{D^2}} \right] \\
&\times \int_0^{2\pi} d\varphi \exp\left\{-\frac{1}{2}D_R(\rho, \varphi)\right\} \quad (1) \\
&\times \cos\left[\frac{k}{f}r\rho \cos(\varphi - \theta)\right],
\end{aligned}$$

where $D_R(\rho, \varphi)$ is the structure function of the residual phase in the polar coordinates ρ and φ , k is the wavenumber, f is the focal length of the telescope, D is the telescope diameter, and r and θ are the modulus and the polar angle of the vector \mathbf{r} , respectively.

For the case of Kolmogorov turbulence the structure function of the residual phase D_R can be expressed as (Voitsekhovich & Bara 1999):

$$\begin{aligned}
D_R(\rho, \varphi) &= 5.83 k^2 \int_0^L dz C_n^2(z) \quad (2) \\
&\times \left[\rho^{5/3} + (\gamma z)^{5/3} - \frac{1}{2}r_+^{5/3} - \frac{1}{2}r_-^{5/3} \right],
\end{aligned}$$

where γ denotes the angular separation between the guide and observed stars, z is the distance in the propagation direction and $r_{\pm} = \sqrt{\rho^2 + \gamma^2 z^2 \pm 2\rho\gamma z \cos\varphi}$.

From Eq. (1) it is easy to get the long-exposure Strehl ratio S_R for the case of a perfect on-axis adaptive correction. This parameter can be expressed as

$$\begin{aligned}
S_R &= \frac{16}{\pi} \int_0^1 d\rho \rho \left(\arccos \rho - \rho \sqrt{1 - \rho^2} \right) \\
&\exp\left[-\frac{1}{2}D_{S_R}(\rho D)\right]. \quad (3)
\end{aligned}$$

In Eq. (3) D is the telescope diameter, and D_{S_R} denotes the structure function of the residual phase given by

$$\begin{aligned}
D_{S_R}(r) &= 5.83 k^2 \int_0^\infty dz C_n^2(z) \\
&\times \left\{ r^{5/3} + (\gamma z)^{5/3} - (r + \gamma z)^{5/3} \right. \\
&\times \left. {}_2F_1\left[-\frac{5}{6}, \frac{1}{2}, 1; \frac{4r\gamma z}{(r + \gamma z)^2}\right] \right\}, \quad (4)
\end{aligned}$$

where $C_n^2(z)$ is the vertical profile of the refractive index structure constant and ${}_2F_1$ denotes the Gauss hyper-geometric function. This structure function is a particular case of Eq. (2) obtained by integrating over the azimuthal angle φ .

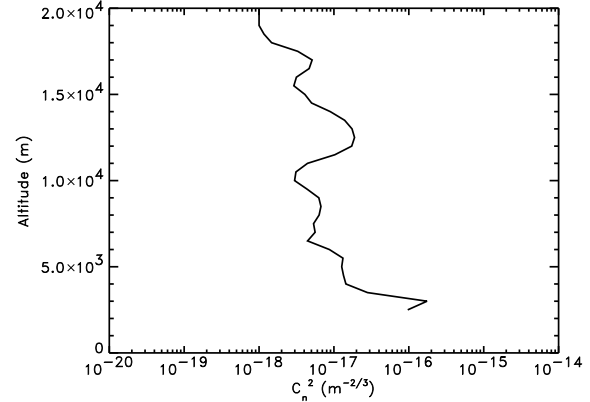


Fig. 1. San Pedro Mártir experimental C_n^2 profile from Generalized Scidar data. The corresponding Fried parameter is 16 cm (for wavelength centered at $0.55 \mu\text{m}$).

3. MEASURED C_n^2 PROFILES

3.1. Generalized Scidar technique

Avila et al. (1997, 1998) presented the first experimental implementation and results of the Generalized Scidar (G-SCIDAR), the concept of which was introduced by Fuchs (1995) and Fuchs, Tallon & Vernin (1998), as an improvement of the known Scidar technique (Rocca et al. 1974). For completeness, we give here a brief overview of the G-SCIDAR data acquisition.

The experimental C_n^2 profile used here (Fig. 1) is the median of 800 profiles obtained during three nights in April 1997 at the 2.1-m telescope of San Pedro Mártir observatory, Baja California, México. A detailed description of this observing campaign is presented by Avila et al. (1998). The data reduction consists of computing the spatial autocorrelation function of short exposure-time images of the scintillation pattern which is produced by a double star detected on a virtual plane a few kilometers beneath the pupil. A maximum entropy algorithm is used to retrieve the C_n^2 profile from the measured autocorrelation function.

The altitude resolution of G-SCIDAR profiles is proportional to the angular separation of the observed double star. The profile used here is obtained from the observation of double stars with different separations, resulting in an average altitude resolution of approximately 500 m.

3.2. Instrumented balloon technique

The acquisition of balloon data involves the launching of meteorological balloons equipped with sensors which measure the microstructure of the thermal field during their free-flight ascent. They

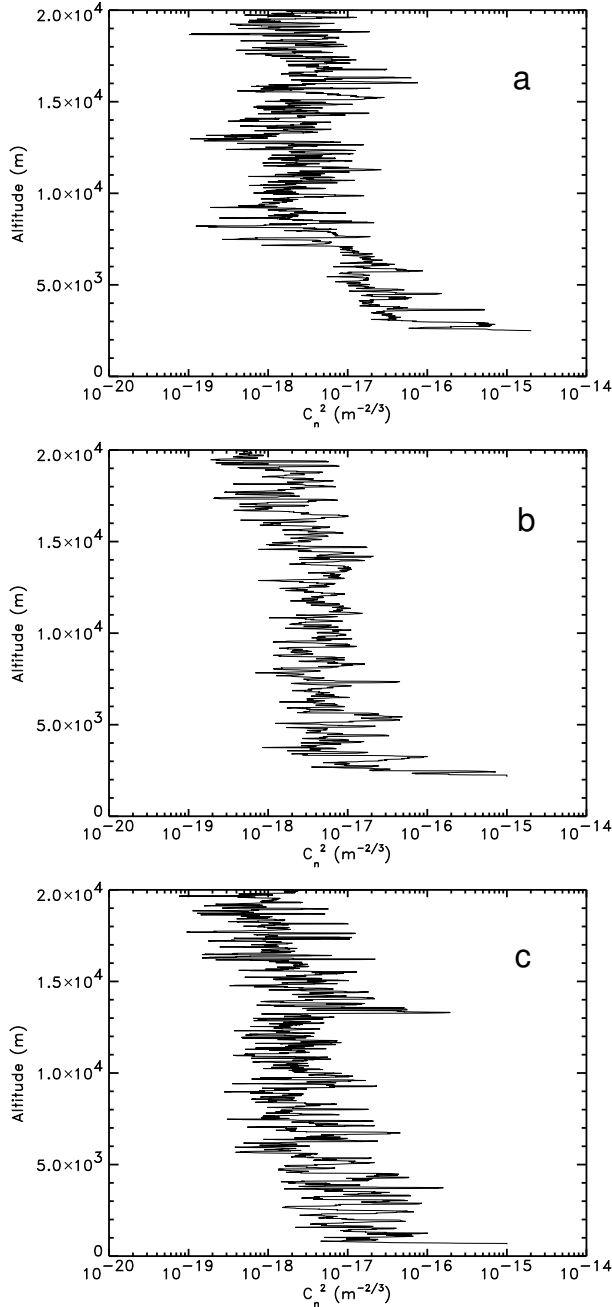


Fig. 2. Experimental C_n^2 profiles from balloon data, obtained at (a) ESO Paranal 16/06/92, (b) ORM, Canary Island 03/11/95, (c) OHP, France 29/9/97. The calculated Fried parameter in cm (at $\lambda = 0.55 \mu\text{m}$) for each site profile is: 17.0, 5.0, and 10.3, respectively

sample the atmosphere from the ground level up to about 25 km.

The temperature structure function is defined as

$$D_T(r) = \langle (T(x) - T(x+r))^2 \rangle, \quad (5)$$

and assessed by means of a couple of sensors sepa-

rated by a distance r . One can deduce the temperature structure constant profile $C_T^2(z)$ by

$$D_T(r, z) = C_T^2(z) r^{2/3}. \quad (6)$$

C_T^2 and C_n^2 can be linked by virtue of the known mean pressure and temperature, P and T , which are also measured on board:

$$C_n^2(z) = C_T^2(z) \left[80 \times 10^{-6} \frac{P(z)}{T(z)^2} \right]^2. \quad (7)$$

The statistical computation of the structure function is performed electronically on board, and in real time during the flight. The structure function is simultaneously calculated for two distinct separations (0.3 and 0.95 m). In doing so, two independent estimates of $C_n^2(z)$ are obtained. The electronic computation on board is able to transmit time, pressure, temperature and humidity R_h . At a 1.5 s duty cycle, the whole set of information is sent to a ground receiver. The ascent speed being of the order of 4 m s^{-1} , the effective vertical resolution is 6 m. We thus have at each 6 m height interval, $D_T(0.3 \text{ m}, h)$, $D_T(0.95 \text{ m}, h)$, P , T , R_h .

From all of these measurements one can obtain a set of extremely valuable astrophysical and geophysical parameters, among these the C_n^2 profile. In Fig. 2 we present three of the four C_n^2 profiles used for our efficiency calculation.

It has been shown that both techniques provide very similar results (Avila et al. 1997, Avila et al. 2002), but G-SCIDAR measurements are significantly cheaper and easier to perform.

3.3. Profile description

All the profiles have a maximum C_n^2 value at ground level, but each shows different features. The median profile obtained at OAN-SPM (Fig. 1) shows an important layer centered at 12.5 km. The value of r_0 , for a wavelength $\lambda = 0.55 \mu\text{m}$ (hereafter, r_0 will always be given for $\lambda = 0.55 \mu\text{m}$), corresponding to that profile is 16.0 cm. The profile in Fig. 2a has a similar r_0 value (17.0 cm), and shows a concentration of the turbulence within the first 7 km (above sea level). In Fig. 2b, the turbulence seems more uniformly distributed and leads to $r_0 = 5.0$ cm, which is the smallest value among the four encountered in this paper. Finally, the profile in Fig. 2c has a very strong layer close to 13 km, and a corresponding r_0 value of 10.3 cm.

4. PSF QUALITATIVE RESULTS

To give the reader some insight to the anisotropic imaging effect, we show here some related pictures

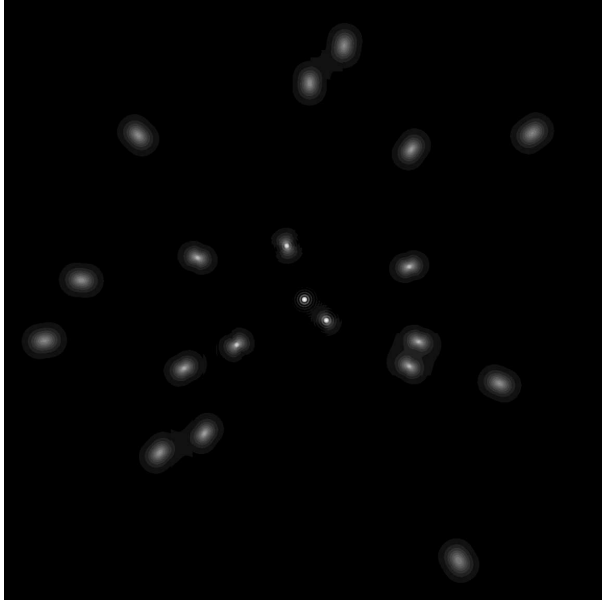


Fig. 3. Example of wide-field adaptive optics image in the visible ($\lambda = 550$ nm, field size is equal to 25×25 arcsec, logarithmic intensity scale, the guide star is located at the center of the picture).

while in the next section we present the corresponding quantitative analysis.

In order to illustrate how the effect of interest can affect the results of wide-field astronomical observations, we show in Fig. 3 an example of 25×25 arcsec long-exposure image of point sources to be obtained after adaptive correction. The PSFs were calculated from Eq. (1) for the V-band ($\lambda = 550$ nm). Note that the stars positions have been chosen randomly, and the guide star is located at the center of the picture. As one can see from Fig. 3, the PSFs have complex shapes which vary considerably with the star position.

To demonstrate the PSF dependence on the wavelength, we show in Fig. 4 the same stars in the J-band ($\lambda = 1250$ nm). As one can see, the anisotropic effect in the infrared is weaker than in the visible, but it is still quite pronounced.

5. QUANTITATIVE ANALYSIS OF THE PSF SHAPE

As one can notice from Figs. 3 and 4, the PSF has a complex shape that depends strongly on the star location. Looking carefully at the pictures, one can distinguish the circular, oval-like or butterfly-like shapes of PSF isophotes. It is interesting to investigate more carefully how the isophotes depend on the PSF level and star separation. A convenient and practical characteristic of the PSF shape is its

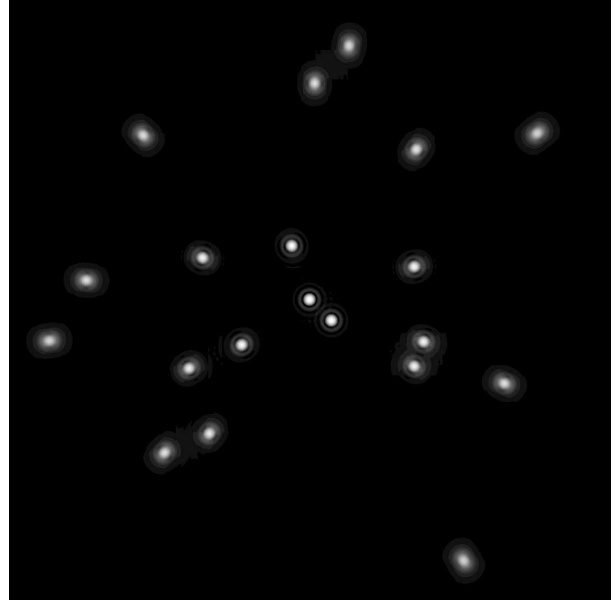


Fig. 4. Example of wide-field adaptive optics image in the near infrared ($\lambda = 1250$ nm, field size is equal to 25×25 arcsec, logarithmic intensity scale, the guide star is located at the center of the picture).

elongation (Close et al. 1998, Voitsekovich & Bara 1999) for a given PSF level, because this parameter can be measured directly in an experiment. Mathematically the elongation is expressed as a ratio of PSF's maximum width to the minimum one at a given level of PSF (Voitsekovich & Bara 1999), and it depends on many parameters: the star separation, the wavelength, the telescope size, etc.

The PSF level versus elongation is plotted in Fig. 5 for several star separations ($\lambda = 550$ nm). One can see a strong dependence of the elongation on the PSF level. One can also notice that the level corresponding to the maximum elongation increases as the star separation increases. This effect is shown in more detail in Fig. 6 where we plot the level of maximum elongation versus star separation. On the other hand, the maximum elongation decreases with the increase of star separation, as shown specifically in Fig. 7.

Another practically important problem related with anisotropic imaging is the width of the anisotropic image. When the image has rotational symmetry, there is no problem to define this width. For example, it can be defined as a radius of the curve encircling 87% of the total image energy. For the case of an anisotropic image, we can use a similar criterion but defining two image parameters: the maximum PSF width r_{\max} (toward the direction of the guide star), and the minimum PSF width r_{\min}

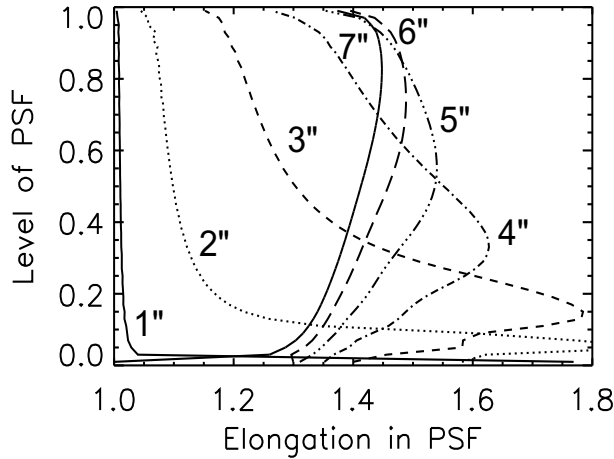


Fig. 5. PSF level versus PSF elongation for several star separations ($\lambda = 550$ nm). The star separations in arcseconds are indicated inside the graph.

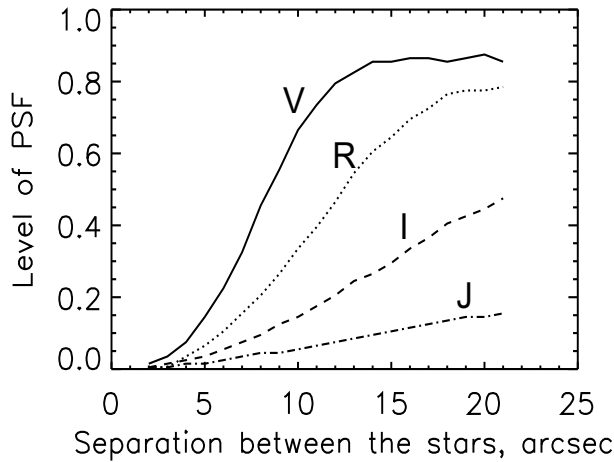


Fig. 6. Level of the maximum elongation versus star separation for different wavelengths. The wavelength bands are indicated inside the graph.

(in the transversal direction). The parameters r_{\max} and r_{\min} are plotted in Figs. 8 and 9 versus star separation for different wavelengths.

6. COMPARISON OF EFFICIENCY

Strehl ratio calculations have been performed for 8-meters-class telescopes because the telescopes of this class are either already operating, under construction or planned to be built. The efficiency of off-axis correction is presented for three bands (V, J, K) centered at 0.55, 1.25 and 2.2 μm which are of interest for observers.

Fig. 10 shows the Strehl ratio for different sites versus the angular separation between the reference and observed object. Since the calculations have been made for the case of perfect adaptive correction,

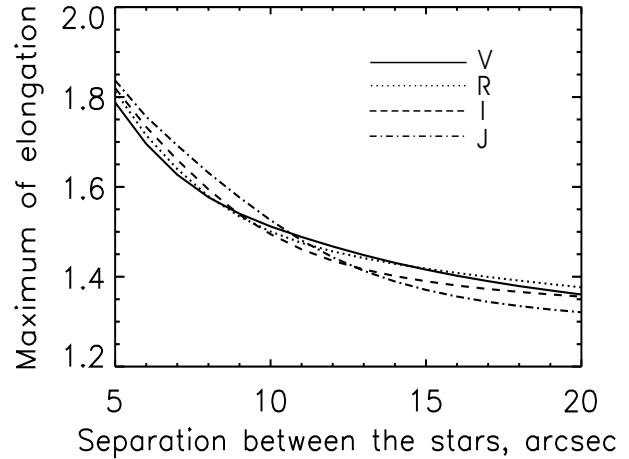


Fig. 7. Maximum elongation versus star separation for different wavelengths. The wavelength bands are indicated inside the graph.

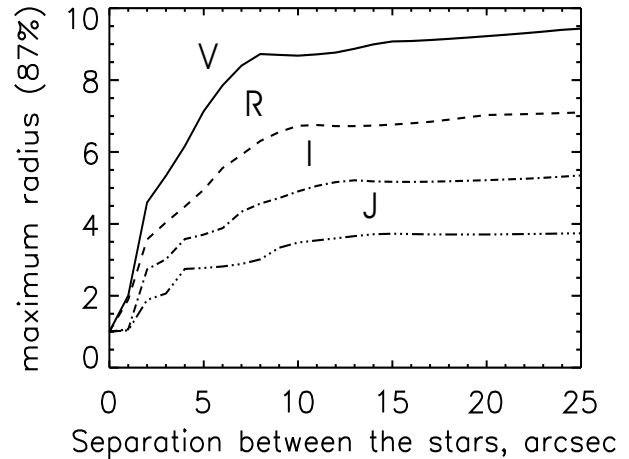


Fig. 8. Maximum PSF width versus star separation for different wavelengths. The wavelength bands are indicated inside the graph.

the graphs present an upper limit of the efficiency that can be reached with a real adaptive system.

One can see from Fig. 10 that the quality of off-axis adaptive correction is quite different for the four considered sites. This effect appears due to a significant difference in the turbulence profiles. As it follows from Eq. 4, the quality of off-axis correction is mainly affected by the quantity $\int_0^L dz z^{5/3} C_n^2(z)$. So, speaking in general terms, the profiles with a turbulence strength concentrated mainly near the ground give better results. Comparing the results presented in Fig. 10, one can conclude that the quality of off-axis correction can differ strongly (up to several times) from one observatory to another.

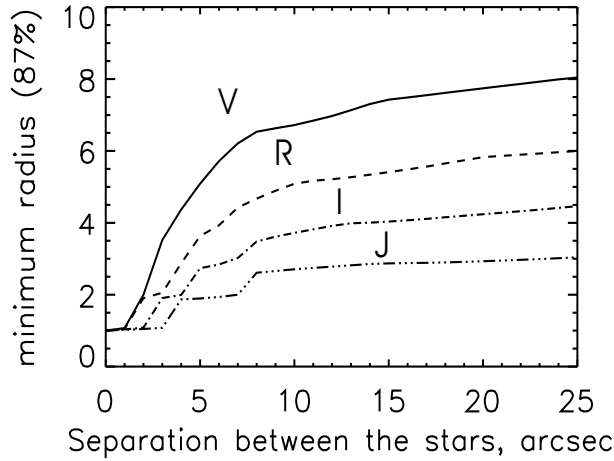


Fig. 9. Minimum PSF width versus star separation for different wavelengths. The wavelength bands are indicated inside the graph.

7. CONCLUSIONS

The shape of the off-axis AO PSF, which mainly depends on the C_n^2 profile, is analyzed by numerical simulations. We based our calculations on the median experimental C_n^2 profile obtained with a Generalized Scidar at the Observatorio Astronómico Nacional at San Pedro Mártir (México)(Avila *et al.* 1998). Using this technique, the shape of the PSF can be calculated for any object at different positions in the field of view. Obtaining a general shape of the PSF on a wide field can be useful in deconvolution algorithms. This shape is also strongly related to the Strehl ratio. In this work we proceeded to compare the calculated efficiency of off-axis AO systems estimated for different turbulence profiles obtained at four astronomical sites, respectively: European Southern Observatory in Paranal, Chile; Observatorio de Roque de los Muchachos, Canary Islands, Observatorio Astronómico Nacional de San Pedro Mártir, México, and two profiles for the Observatoire de Haute Provence, France. The efficiency of interest is considered through the Strehl ratio of the corrected image calculated for V, J, and K bands and for 8-m class telescopes. It is found that this efficiency depends mainly on the C_n^2 profile layered structure and on the turbulence strength. Among the compared sites, our results suggest that one can expect the best quality of off-axis adaptive correction at OAN-SPM. However, this conclusion is only preliminary, since more data is required for a statistical study. We are planning to carry out more complete C_n^2 data analysis and measurements at SPM.

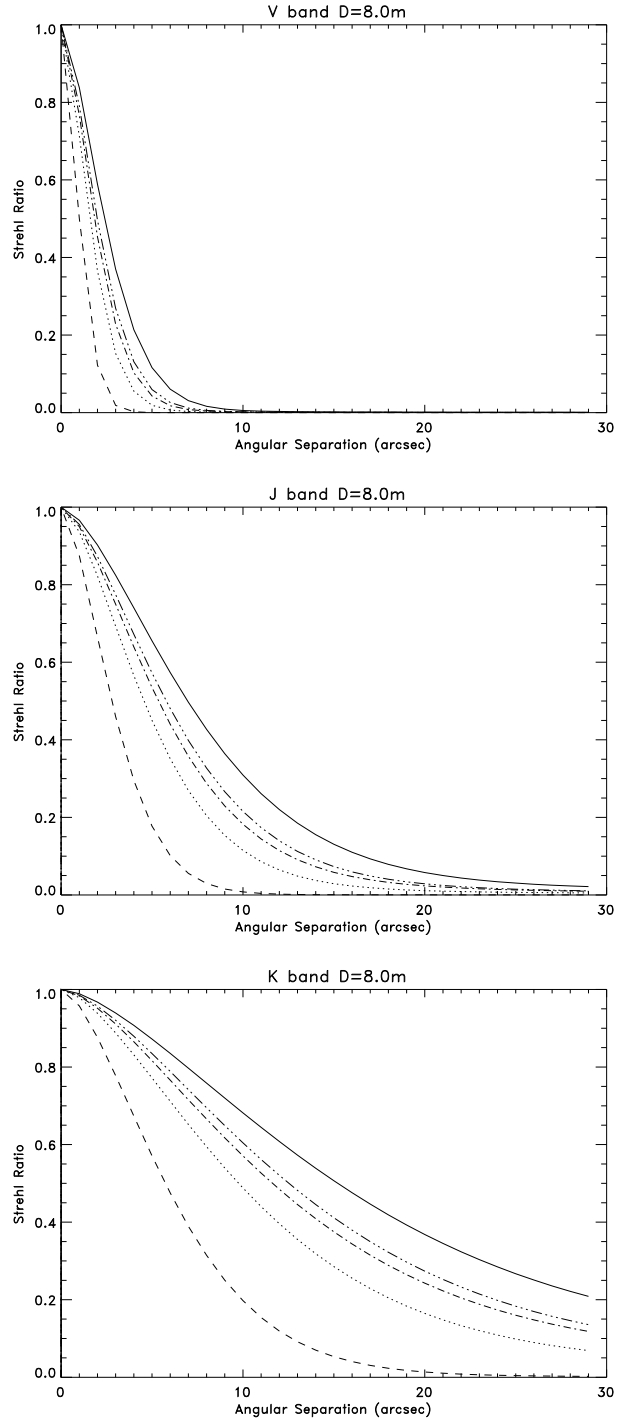


Fig. 10. Strehl ratio versus the angular separation between the stars for 8.0m telescope. a) V band, b) J band and c) K band. Lines coding is: Observatorio Astronómico Nacional at San Pedro Mártir, México (continuous line), ESO Paranal, Chile (dotted line), Observatorio de Roque de los Muchachos, Canary Islands (dashed line), Observatoire de Haute Provence, France (i) (dotted-dashed line) and (ii) (3 dots-dashed line).

We are indebted to J. Vernin and M. Azouit from University of Nice (France) Astrophysics Department for kindly providing balloon data used in this investigation. This work was partially supported by ECOS-ANUIES-CONACYT grant M97U01. L. J. Sánchez and R. Avila received support from Consejo Nacional de Ciencia y Tecnología (México) projects 400354-5-I29854E and J32412E, respectively.

REFERENCES

- Avila, R., Vernin, J., & Masciadri, E. 1997, *Appl. Opt.*, 36, 7898
- Avila, R., Vernin, J., & Cuevas, S. 1998, *PASP*, 110, 1106
- Avila, R., Vernin, J., Azouit, M., Agabi, A., Sánchez, L. J., Masciadri, E., Cuevas, S., Garfias, F., Harris, O., Voitsekhovich, V., & Orlov, V. 2002, in *ASP Conf. Ser.*, 266, “Astronomical Site Evaluation in the Visible and Radio Range”, eds. J. Vernin, Z. Benkhaldoun and C. Muñoz-Tuñón (San Francisco: ASP), 484
- Close, L. M., Roddier, F. J., Roddier, C. A., Graves, J. E., Northcott, M. J., and Potter, D. 1998 *Proc. SPIE* 3353, 406
- Chassat, F. 1989, *J. Optics (Paris)*, 20, 13
- Fusco, T., Conan, J.-M., Mugnier, L. M., Michau, V., & Rousset, G. 2000, *A&AS*, 142, 149
- Fuchs, A. 1995, Ph. D. thesis (Université de Nice-Sophia Antipolis)
- Fuchs, A., Tallon, M., & Vernin, J. 1998, *PASP*, 110, 86
- Vitrichenko, E. A., Voitsekhovich, V. V., & Mishchenko, M. I. 1984, *News of Academy of Sciences USSR: Atmospheric and Oceanic Optics*, 20-9, 870
- Voitsekhovich, V. V., Orlov, V. G., Cuevas, S. & Avila, R. 1998, *A&AS*, 133, 427
- Voitsekhovich, V. V., & Bara, S. 1999, *A&AS*, 137, 385

Remy Avila: Centro de Radioastronomía y Astrofísica, Universidad Nacional Autónoma de México, Apartado Postal 3-72, 58090 Morelia, Michoacán, México (r.avila@astrosmo.unam.mx).

Valeri Orlov, Leonardo Sánchez, Valerii Voitsekhovich: Instituto de Astronomía, Universidad Nacional Autónoma de México, Campus CU, Apdo. Postal 70-264, Cd. Universitaria, 04510 México D.F., México (orlov,leonardo,voisteko@astroscu.unam.mx).